

Gamma-ray Emission from Pulsar Outer Magnetospheres

K. Hirotani

National Astronomical Observatory, Mitaka, Tokyo 181-8588, Japan

Abstract. We study the γ -ray emission from an outer-gap accelerator around a rotating neutron star. Assuming the existence of global currents in the magnetosphere, the charge depletion causes a large electric field along the magnetic field lines. This electric field accelerates migratory electrons and positrons which radiate gamma-rays via curvature radiation. These gamma-rays, in turn, produce yet more radiating particles by colliding with the X-rays, leading to a pair-production cascade. Imposing a gap-closure condition that a single pair produces one pair in the gap, on average, we explicitly solve the strength of the acceleration field and demonstrate how the peak energy and the luminosity of the curvature-radiated GeV photons and the cutoff energy and luminosity of Compton-scattered TeV photons depend on such parameters as the surface temperature, the rotational frequency, and the magnetic moment. It is demonstrated that both the GeV and TeV emissions of Geminga will be harder than those of B1055-52, B0656+14, and Vela, and that the TeV fluxes are too small to be observed by current ground-based telescopes.

1. Introduction

The EGRET experiment on the *Compton Gamma Ray Observatory* has detected pulsed signals from at least six rotation-powered pulsars, which are known traditionally as radio pulsars. Interpreting γ -rays should be less ambiguous than interpreting nonthermal X-rays. Therefore, γ -rays are particularly important as a direct signature of basic nonthermal processes in pulsar magnetospheres and potentially should help to discriminate among different emission models.

Attempts to model the γ -ray emission have concentrated on two scenarios: polar-cap models with emission altitudes within several neutron-star radii over a polar-cap surface (Harding, Tadamaru, & Esposito 1978; Daugherty & Harding 1982, 1996; Sturmer, Dermer, & Michel 1995) and outer-gap models with acceleration occurring in the open-field zone located near the light cylinder (Cheng, Ho, & Ruderman 1986a,b, hereafter CHR; Chiang & Romani 1992, 1994). Recently, Romani (1996) described an emission model for γ -ray pulsars based on curvature-radiation–reaction–limited charges and estimated the efficiency of GeV photon production as a function of pulsar age, magnetic field strength, and magnetic inclination α_i .

However, in order to understand the γ -ray emission mechanism, the acceleration field, $E_{||}$, in the gap is crucial. It was Hirotani & Shibata (1999a,b, hereafter Papers I, II) who first solved the spatial distribution of $E_{||}$ together

with particle and γ -ray distribution functions. They explicitly demonstrated that the outer gap is formed around the null surface where the local Goldreich-Julian charge density $\rho_{GJ} = \Omega B_z / (2\pi c)$ vanishes, where B_z is the component of the magnetic field along the rotation axis. If the transfield thickness of the gap, D_\perp , is comparable with or greater than the longitudinal half-width, H , then E_\parallel is distributed quadratically, having the peak at the null surface.

In this paper, instead of solving the spatial distribution of E_\parallel , we represent its value near the center of the gap. By imposing a gap-closure condition that a single pair produces one pair in the gap on average, we demonstrate how the peak energy and the luminosity of γ -rays depend on the parameters such as the rotation, magnetic moment, and surface temperature.

In the next section, we consider the gap-closure problem and derive the equation that describes H . Using the solutions of H , we investigate general γ -ray emission properties in §3. We apply the theory to three middle-aged pulsars in §4. In the final section, we discuss the validity of assumptions and consider the difference from the model of Zhang & Cheng (1997), who considered another gap-closure condition where H is regulated so that the curvature-radiated γ -ray energy is adjusted just above the threshold for pair production.

2. Structure of the Gap

2.1. Vacuum Acceleration Field

It is demonstrated in Paper I that the structure of the gap along the magnetic field lines is symmetric with respect to the null surface if the transfield thickness of the gap is large in the sense of $D_\perp > H$. In this paper, we consider such a one-dimensional gap by introducing rectilinear coordinates: x is an outwardly increasing coordinate along the magnetic field lines, while z is parallel to the rotational axis. We define $x = 0$ to be the intersection between the last open field line and the null surface where $B_z = 0$ (Figure 1). Supposing the magnetic fields to be straight lines along x , and approximating the null surface to be at the z -axis, we can Taylor-expand ρ_{GJ} around $x = 0$ to obtain the following Poisson equation for the non-corotational potential, Φ :

$$-\frac{d^2\Phi}{dx^2} = -4\pi Ax, \tag{1}$$

where A denotes the expansion coefficient of ρ_{GJ} at the null surface ($x = 0$). It is of the order of ρ_{GJ}/r_{LC} , where r_{LC} refers to the light-cylinder radius, and is explicitly defined as

$$A \equiv \frac{3\Omega\mu}{2\pi cr_0^4} \left[\frac{3}{2} \sin 2\theta_0 \cos 2(\theta_0 - \alpha_i) + \cos 2\theta_0 \sin(\theta_0 - \alpha_i) \right], \tag{2}$$

where μ refers to the magnetic dipole moment of the neutron star and c is the velocity of light. The position (r_0, θ_0) in polar coordinates indicates the center of the gap ($x = 0$). They are given by

$$\frac{r_0}{r_{LC}} \equiv \frac{4}{4 + \tan^2 \theta_0} \frac{2 \tan^2 \alpha_i + 3 + \sqrt{9 + 8 \tan^2 \alpha_i}}{(4/3) \tan^2 \alpha_i + 3 + \sqrt{9 + 8 \tan^2 \alpha_i}}, \tag{3}$$

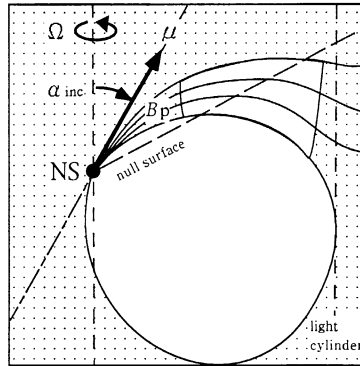


Figure 1. A side view of a hypothetical outer magnetospheric gap.

$$\tan \theta_0 \equiv \frac{3 \tan \alpha_i + \sqrt{9 \tan^2 \alpha_i + 8}}{2}. \tag{4}$$

As a typical inclination, we adopt $\alpha_i = 30^\circ$ in this paper. We then obtain $A = 2.8 \times 10^{-12} \Omega_2^5 \mu_{30}$, $r_0 = 0.40 r_{LC}$, and $\theta_0 = 68^\circ$, where $\Omega_2 \equiv \Omega/10^2 \text{ rad s}^{-1}$ and $\mu_{30} \equiv \mu/10^{30} \text{ G cm}^3$. In terms of Ω_2 , r_{LC} can be given by $r_{LC} = 3.0 \times 10^8 \Omega_2^{-1} \text{ cm}$.

Integrating Equation (1), we obtain the acceleration field $E_{||} \equiv -d\Phi/dx = E_{||}(0) - 2\pi Ax^2$, where $E_{||}(0)$ refers to the value of $E_{||}$ at $x = 0$. Defining the boundaries of the gap to be the places where $E_{||}$ vanishes, we obtain $E_{||}(0) = 2\pi AH^2$. We can evaluate the typical strength of $E_{||}$ by averaging its values throughout the gap as follows:

$$\begin{aligned} E_{||} &= \frac{1}{H} \int_0^H dx (E_{||}(0) - 2\pi Ax^2) = \frac{4}{3} \pi AH^2 \\ &= 3.1 \times 10^{10} \Omega_2^3 \mu_{30} \left(\frac{H}{r_{LC}} \right)^2 \frac{\text{V}}{\text{m}}. \end{aligned} \tag{5}$$

In the last line, we substitute $A = 2.8 \times 10^{-12} \Omega_2^5 \mu_{30} \text{ esu}$, assuming $\alpha_i = 30^\circ$.

2.2. Pair-Production Mean Free Path

The most effective assumption for the particle motion in the gap arises from the fact that the velocity saturates immediately after their birth in the balance between the radiation-reaction force and the electric force. The reaction force is mainly due to curvature radiation if the gap is embedded in a moderate, surface X-ray field. (For younger pulsars such as Crab, the inverse-Compton process becomes the dominant process.) Equating the electric force $eE_{||}$ and the radiation-reaction force, we obtain the saturated Lorentz factor at each point,

$$\Gamma = \left(\frac{3R_c^2 E_{||}}{2e} \right)^{1/4} = 9.2 \times 10^7 (R_{0.5}^2 \Omega_2 \mu_{30})^{1/4} \left(\frac{H}{r_{LC}} \right)^{1/2}, \tag{6}$$

where $R_{0.5}$ is the curvature radius R_c divided by $0.5r_{LC}$ and e refers to the magnitude of the charge on the electron. In the second line, we assumed $\alpha_i = 30^\circ$. Using this Γ , we obtain the central energy of curvature radiation,

$$E_c = \frac{3\Gamma^3 hc}{4\pi R_c} = 155 \left(R_{0.5}^2 \Omega_2^7 \mu_{30}^3 \right)^{1/4} \left(\frac{H}{r_{LC}} \right)^{3/2} \text{ GeV}, \tag{7}$$

where h is the Planck constant. In the second line, we assumed $\alpha_i = 30^\circ$. In this paper, we adopt the gray approximation in the sense that all the γ -rays are radiated at energy E_c .

Let us next consider how the X-ray field determines the pair-production mean free path. First, equation (7) gives the threshold energy for soft photons to materialize as pairs by colliding with the γ -rays having energy $m_e c^2 \epsilon_\gamma = E_c$,

$$E_{th} = \frac{2}{1 - \mu_c} \frac{m_e c^2}{\epsilon_\gamma}, \tag{8}$$

where μ_c refers to the cosine of the three-dimensional collisional angle between the γ -rays and the X-rays.

To evaluate μ_c , we first consider the γ -rays' toroidal momenta due to aberration. At the gap center, the aberration angle ϕ_{abb} is given by $\tan^{-1}(r_0 \sin \theta_0 / r_{LC})$. In the case of $\alpha_i = 30^\circ$, we obtain $\phi_{abb} = 20.4^\circ$. In this case, the collisional angle on the poloidal plane becomes $\theta_c = 90^\circ - \theta_0 = 21.6^\circ$ (or $\theta_c = 90^\circ + \theta_0 = 158.4^\circ$) for outwardly (or inwardly) propagating γ -rays. We thus obtain $\mu_c = \cos \phi_{abb} \sin \theta_c = \pm 0.345$, where the upper and the lower sign correspond to the outwardly and inwardly propagating γ -rays, respectively. The value of μ_c does not change very much from this value for $\alpha_i > 30^\circ$, because the effect of aberration due to the toroidal motion prevents μ_c from becoming very large even if the collision angles on the poloidal plane become very small. On these grounds, we adopt $\mu_c = \pm 0.345$ as a representative value for $\alpha_i = 30^\circ$.

On these grounds, assuming $\alpha_i = 30^\circ$, we can rewrite equation (8) into

$$E_{th} = \frac{3.4}{1 - \mu_c} \left(R_{0.5}^2 \Omega_2^7 \mu_{30}^3 \right)^{-1/4} \left(\frac{H}{r_{LC}} \right)^{-3/2} \text{ eV}. \tag{9}$$

Let us consider the pair-production mean free path, λ_s , for a γ -ray photon to materialize in a collision with one of the soft blackbody X-rays. If only outwardly propagating γ -rays were to contribute to λ_s , it would be given by

$$\lambda_s^{-1} \equiv \int_{2/(1-\mu_c)\epsilon_\gamma}^{\infty} d\epsilon_x \frac{dN_s}{d\epsilon_x} \sigma_p(\epsilon_\gamma, \epsilon_x, \mu_c), \tag{10}$$

where $\mu_c = 0.345$ and the pair-production cross-section is given by

$$\sigma_p(\epsilon_\gamma, \epsilon_x, \mu_c) \equiv \frac{3}{16} \sigma_T (1 - v^2) \left[(3 - v^4) \ln \frac{1 + v}{1 - v} - 2v(2 - v^2) \right], \tag{11}$$

$$v(\epsilon_\gamma, \epsilon_x, \mu_c) \equiv \sqrt{1 - \frac{2}{1 - \mu_c} \frac{1}{\epsilon_\gamma \epsilon_x}}; \tag{12}$$

σ_T is the Thomson cross section, and $\epsilon_x \equiv E_x/m_e c^2$ refers to the nondimensional energy of an X-ray photon. We may notice here that the nondimensional threshold energy ($E_{th}/m_e c^2$) appears in the lower bound of the integral. The spectrum of the soft blackbody component is given by the Planck law

$$\frac{dN_s}{d\epsilon_x} = 2\pi \left(\frac{m_e c^2}{ch} \right)^3 \left(\frac{A_s}{4\pi r_0^2} \right) \frac{\epsilon_x^2}{\exp(\epsilon_x/\Delta_s) - 1}, \quad (13)$$

where A_s indicates the observed radius of the blackbody emitting region; Δ_s is defined by

$$\Delta_s \equiv \frac{kT_s}{m_e c^2}, \quad (14)$$

where kT_s refers to the soft blackbody temperature measured by a distant observer. Since the outer gap is located outside of the deep gravitational potential well of the neutron star, the photon energy there is essentially the same as what the distant observer measures.

In a realistic outer gap, not only the outwardly propagating γ -rays but also the inwardly propagating ones contribute to λ_s . Therefore, we compute λ_s by taking an arithmetic average as follows:

$$\begin{aligned} \frac{1}{\lambda_s} &\equiv \kappa \int_{2/(1-\mu_c)\epsilon_\gamma}^{\infty} d\epsilon_x \frac{dN_s}{d\epsilon_x} \sigma_p(\epsilon_\gamma, \epsilon_x, \mu_c) + \\ &+ (1-\kappa) \int_{2/(1-\mu_c)\epsilon_\gamma}^{\infty} d\epsilon_x \frac{dN_s}{d\epsilon_x} \sigma_p(\epsilon_\gamma, \epsilon_x, \mu_c). \end{aligned} \quad (15)$$

The first (or second) term represents the contribution from the outwardly (or inwardly) propagating γ -rays; we thus adopt $\mu_c = 0.345$ (or -0.345) for $\alpha_i = 30^\circ$. The weight κ reflects the ratio of fluxes between the outwardly and inwardly propagating γ -rays. For example, if κ were to be 1.0, only outward γ -rays would contribute to pair production. Since we know that the flux of the outward γ -rays is typically about ten times larger than that of inward ones (Paper III), we adopt $\kappa = 0.9$ in this paper.

In the present paper, we are mainly concerned with cooling neutron stars. Thus, the background radiation field is considered to be dominated by the surface blackbody component. However, to take account of the effect of the hard X-ray components such as the heated polar-cap emission, we compute the mean free path, λ_p , for the pair production as follows (Beskin, Istomin, & Par'ev 1992):

$$\frac{1}{\lambda_p} = \frac{1}{\lambda_s} + \frac{1}{\lambda_h}, \quad (16)$$

where λ_h is obtained in the same manner as λ_s by replacing kT_s with the temperature of the heated polar cap, kT_h , and A_s with the observed area of the hard component, A_h .

2.3. Gap Closure

The gap width $2H$ is adjusted so that a single pair produces copious γ -ray photons (of number N_γ), one of which materializes as a pair, on average. Therefore,

the probability of a γ -ray photon materializing within the gap, N_γ^{-1} , must coincide with the optical depth for absorption, $2H/\lambda_p$. The gap closure is, therefore, realized if

$$2H = \lambda_p/N_\gamma \quad (17)$$

is satisfied, where

$$N_\gamma \approx \frac{2H}{c} \frac{4\pi e^2 \Gamma}{9hR_c} = 6.0 \times 10^5 \left(\frac{\Omega_2 \mu_{30}}{R_{0.5}^2} \right)^{1/4} \left(\frac{H}{r_{LC}} \right)^{3/2}. \quad (18)$$

It follows that the optical depth for pair production, N_γ , is much greater than unity. Substituting Equations (18) and (16) into (17), we finally obtain the equation which describes H/r_{LC} as a function of B_5 , Ω_2 , kT_s , A_s , kT_h , and A_h .

2.4. Gamma-ray Luminosity

Let us consider the luminosities of curvature-radiated and inverse-Compton-scattered γ -rays. First, the former luminosity, L_{GeV} , can be estimated by multiplying the total number of positrons and electrons in the gap, N_e , the number of γ -rays emitted per particle per unit time, $N_\gamma/(2H/c)$, and γ -ray energy, E_c . That is, we have

$$L_{GeV} = N_e \times \frac{N_\gamma}{2H/c} \times E_c. \quad (19)$$

Evaluating the conserved current density by $\chi c \rho_{GJ} = \chi(\Omega B/2\pi e)$, we obtain

$$N_e \sim \chi \cdot \frac{\Omega B}{2\pi c e} (2\pi r_0 \sin \theta_0) D_\perp H. \quad (20)$$

The distance of the gap center from the rotation axis, $r_0 \sin \theta_0$, becomes $0.37r_{LC}$ for $\alpha_i = 30^\circ$. Substituting Equations (7), (18), and (20) into (19), we obtain

$$L_{GeV} \sim 2.0 \times 10^{39} \chi \left(\frac{D_\perp}{r_{LC}} \right) \Omega_2^4 \mu_{30}^2 \left(\frac{H}{r_{LC}} \right)^3 \text{ erg s}^{-1}. \quad (21)$$

In Papers I, II, and III, it is demonstrated that stationary solutions exist even when D_\perp becomes comparable with r_{LC} . We thus assume a transversely thick outer gap with $D_\perp = r_{LC}$. If D_\perp is much less than this value, like CHR assumed, the γ -ray luminosity becomes much less than that which would be obtained under $D_\perp = r_{LC}$. As for χ , its maximum values will be about 0.2 for a wide range of the parameters kT_s , Ω , and μ (Papers I, II, III), provided that no particles enter from the boundaries. We thus assume $\chi \sim 0.1$ in this paper.

Second, let us consider the luminosity of Compton-scattered γ -rays, L_{TeV} . We should notice here that it is the infrared photons with energy ~ 0.1 eV that contribute most effectively as the target photons of IC scatterings. Neither the higher energy photons, like surface blackbody X-rays, nor the lower energy photons, like polar radio emission, contribute as much as the target photons because they have either too small cross-sections or too small energy transfer when they are scattered. The collisional frequency for a particle to inversely scatter the infrared photons of number density $N_{0.1eV}$ is given by $cN_{0.1eV}\sigma_T$.

Considering the fact that the maximum energy of the scattered photons is $\Gamma m_e c^2$, we can evaluate the upper limit of the TeV emission as

$$L_{\text{TeV}} < 2N_e \times cN_{0.1\text{eV}}\sigma_T \times \Gamma m_e c^2 \\ = 2.4 \times 10^5 \chi \left(\frac{D_\perp}{r_{\text{LC}}} \right) \Omega_2^{13/4} \mu_{30}^{5/4} R_{0.5}^{1/2} L_{0.1\text{eV}} \left(\frac{H}{r_{\text{LC}}} \right)^{3/2} \text{ erg/s}, \quad (22)$$

where $L_{0.1\text{eV}}$ refers to the luminosity of infrared photons that can be scattered up to TeV energy range. The ratio between L_{TeV} and L_{GeV} then becomes

$$\frac{L_{\text{TeV}}}{L_{\text{GeV}}} < 1.17 \times 10^{-4} L_{30} \left(\frac{R_{0.5}^2}{\Omega_2^3 \mu_{30}^3} \right)^{1/4} \left(\frac{H}{r_{\text{LC}}} \right)^{-3/2}, \quad (23)$$

where $L_{30} \equiv L_{0.1\text{eV}}/10^{30} \text{ erg s}^{-1}$. It follows that TeV luminosities are much less than GeV ones for moderate values of the parameters. The effect of pair production due to TeV-eV photon collisions is, therefore, self-consistently negligible compared with that due to GeV-keV collisions.

3. Gamma-ray Radiation vs. Surface Blackbody Temperature

Once H/r_{LC} is obtained from Equation (17), we can compute all other quantities by using Equations (5)–(18) and (21)–(22). To this aim, we first show the results of H/r_{LC} as a function of kT_s , Ω , and μ in §3.1. We then study the voltage drop in §3.2 and the γ -rays emission in §3.3. Throughout this section, we assume that the X-rays illuminating the gap are emitted from the whole neutron-star surface. Therefore, we neglect the presence of the hard component and put $\lambda_h = \infty$ in Equation (16) and $A_s = A_* \equiv 4\pi r_*^2$ in Equation (13) in this section, where r_* refers to the neutron-star radius and is supposed to be 10 km in this paper.

3.1. Gap Half-width

Solving Equation (17) for H/r_{LC} , we obtain the gap half-width as a function of kT_s . The results are presented in Figure 2. The thick solid, dashed, and dotted lines correspond to $\mu_{30} = 1.0, 3.0,$ and 0.3 with $\Omega_2 = 0.5$, respectively, while the thin dashed and dotted ones correspond to $\Omega_2 = 0.75$ and 0.25 with $\mu = 1.0$. The curvature radius is fixed as $R_{0.5} = 1.0$.

First of all, it follows from the figure that H/r_{LC} is a decreasing function of kT_s . The reason is as follows. If kT_s increases, the number density of target soft photons $N_s(E > E_{\text{th}})$ increases for a fixed value of E_{th} . The increased $N_s(E > E_{\text{th}})$ results in the decrease of λ_p , which reduces H (Equation (17)). For more accurate discussion, we must take account of the fact that the resultant increase of E_{th} and the decrease of N_γ partially cancel the reduction of H . For example, the reduced H results in a decrease of E_{\parallel} and, hence, E_c . This, in turn, increases E_{th} to decrease $N_s(E > E_{\text{th}})$; as a result, λ_p partially increases. In addition, the reduction of H implies a reduction in the emitting length for a particle, thereby decreasing N_γ . Nevertheless, both of the effects are passive; therefore, the nature of the decrease of H with increasing kT_s is unchanged.

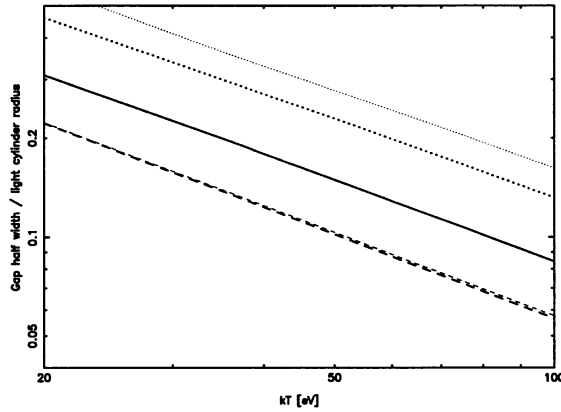


Figure 2. Examples of the gap half-width, H , divided by light-cylinder radius, r_{LC} , as a function of kT_s , Ω , and B . Both the abscissa and the ordinate are in logarithmic scales. The thick solid, dashed, and dotted lines correspond to $(\Omega_2, \mu_{30}) = (1.0, 1.0)$, $(1.0, 3.0)$, and $(1.0, 0.3)$, while the thin dashed and dotted ones correspond to $(0.75, 1.0)$ and $(0.25, 1.0)$, respectively.

From the numerical results, a useful approximated solution can be obtained:

$$\frac{H}{r_{LC}} = 0.0457 \Omega_2^{-0.88} \mu_{30}^{-0.34} \left(\frac{kT_s}{100 \text{ eV}} \right)^{-0.82}. \tag{24}$$

The error is within 5% in the parameter ranges $0.25 < \Omega_2 < 1.0$, $0.3 < \mu_{30} < 3.0$, and $20 < kT_s < 100 \text{ eV}$.

3.2. Acceleration Field and Voltage Drop

The representative value of the acceleration field, $E_{||}$, can be readily computed from Equations (5) and (24). The result is

$$E_{||}(0) = 6.5 \times 10^7 \Omega_2^{1.24} \mu_{30}^{0.32} \left(\frac{kT_s}{100 \text{ eV}} \right)^{-1.64} \frac{\text{V}}{\text{m}}. \tag{25}$$

Thus, the terminal Lorentz factor becomes as large as

$$\Gamma = 2.0 \times 10^7 \Omega_2^{-0.19} \mu_{30}^{0.08} R_{0.5}^{0.5} \left(\frac{kT_s}{100 \text{ eV}} \right)^{-0.41}. \tag{26}$$

The dependences on μ are very small. To sum up, both $E_{||}$ and Γ increase with decreasing kT_s .

Integrating $E_{||}(x) = E_{||}(0) - 2\pi Ax^2$ over x from $-H$ to $+H$, we obtain the voltage drop in the gap:

$$\frac{V_{\text{gap}}}{V_{\text{surface}}} = 5.7 \times 10^{-3} \Omega_2^{-2.6} \mu_{30}^{-1.0} \left(\frac{kT_s}{100 \text{ eV}} \right)^{-2.5}, \tag{27}$$

where V_{surface} ($\sim 10^{15.5} \Omega_2^2 \mu_{30} \text{ V}$) refers to the available voltage drop on the spinning neutron-star surface.

3.3. Curvature Radiation

Let us next consider the energy and luminosity of curvature radiation. Substituting Equation (24) into (7), we obtain

$$E_c = 1.5 \Omega_2^{0.43} \mu_{30}^{-0.57} R_{0.5}^{0.5} \left(\frac{kT_s}{100 \text{ eV}} \right)^{-1.3} \text{ GeV}. \tag{28}$$

As for the luminosity, substituting the results of H/r_{LC} into (21), we obtain the γ -ray luminosity due to curvature radiation as

$$L_{\text{GeV}} = 2.0 \times 10^{34} \left(\frac{\chi}{0.1} \frac{D_{\perp}}{r_{LC}} \right) \Omega_2^{1.36} \mu_{30}^{0.98} \left(\frac{kT_s}{100 \text{ eV}} \right)^{-2.46} \text{ erg s}^{-1}. \tag{29}$$

We can conclude that both the peak energy and the luminosity of the GeV γ -rays are decreasing functions of kT_s . This fact is deeply related to the increase of target X-ray photons for pair production with increasing kT_s .

3.4. Inverse Compton Scatterings

The relativistic particles produce γ -rays mainly via curvature radiation as described in the preceding sections. However, even though energetically negligible, it is useful to draw attention to the TeV γ -rays produced via inverse-Compton (IC) scatterings. Substituting the relation (24) into (22), we obtain the γ -ray luminosity due to IC scatterings as

$$L_{\text{TeV}} < 2.3 \times 10^{32} \left(\frac{\chi}{0.1} \frac{D_{\perp}}{r_{LC}} \right) \Omega_2^{1.93} \mu_{30}^{0.74} R_{0.5}^{0.5} \times \left(\frac{kT_s}{100 \text{ eV}} \right)^{-1.23} \left(\frac{L_{0.1\text{eV}}}{10^{30} \text{ erg s}^{-1}} \right) \text{ erg s}^{-1}. \tag{30}$$

We can see that both the cutoff energy and the luminosity of TeV γ -rays are decreasing functions of kT_s from the same reason as for GeV emission.

4. Application to Individual Pulsars

In this section, we apply the theory to six pulsars. We present in Table 1 their observed X-ray properties in order of spin-down luminosity, \dot{E}_{rot} [erg s^{-1}].

Table 1. Input X-ray field.

pulsar	$\log_{10} \dot{E}_{\text{rot}}$	dist. kpc	Ω rad/s	$\log_{10} \mu$	kT_s keV	A_s/A_*	kT_h keV	A_h/A_*
Vela	36.84	0.50	61.3	30.53	150	0.066
B0656+14	34.58	0.76	15.3	30.67	67	4.5	129	$10^{-1.49}$
Geminga	34.51	0.16	26.5	30.21	48	0.16
B1055-52	34.48	1.53	31.9	30.03	68	7.3	320	$10^{-3.64}$

Substituting the parameters presented in Table 1, we obtain the gap width and the resultant γ -ray emission properties of each pulsar (Table 2). It follows

Table 2. Expected properties of curvature-radiated γ -rays.

pulsar	H/r_{LC}	E_c GeV	L_{GeV} erg s $^{-1}$	$\Gamma m_e c^2$ TeV	L_{TeV}/L_{GeV}
Vela	0.048	1.6	3.1×10^{33}	12.1	$< 7.7 \times 10^{-7} \times L_{30}$
B0656+14	0.16	1.2	1.1×10^{33}	17.5	$< 1.0 \times 10^{-5} \times L_{30}$
Geminga	0.29	3.4	6.4×10^{33}	20.5	$< 3.4 \times 10^{-5} \times L_{30}$
B1055-52	0.13	1.1	6.0×10^{32}	13.2	$< 1.3 \times 10^{-5} \times L_{30}$

from the results of E_c that the GeV spectrum of Geminga should be much harder than those of Vela, B0656+14, and B1055-52. This is because the number density of X-rays at the gap is significantly small for Geminga. From the same reason, the GeV luminosity of Geminga is expected to be large. It is important to note that the TeV emission produced via inverse-Compton scatterings is unobservable from such rotation-powered pulsars. This conclusion is, in fact, general because $L_{TeV} \ll L_{GeV}$ is derived from the general relation (23). The properties of E_c and L_{GeV} will be able to be checked by GLAST, which will help us to discriminate among different models of high-energy emission from pulsar magnetospheres.

Acknowledgments

This research owes much to the helpful comments of Dr. S. Shibata. The author wishes to express his gratitude to Drs. A. Harding and Y. Saito for valuable advice. He also thanks the Astronomical Data Analysis Center of the National Astronomical Observatory, Japan, for the use of workstations.

References

- Beskin, V. S., Istomin, Y. N., & Par'ev, V. I. 1992, *Sov. Astron.*, 36(6), 642
 Cheng, K. S., Ho, C., & Ruderman, M. 1986a, *ApJ*, 300, 500
 Cheng, K. S., Ho, C., & Ruderman, M. 1986b, *ApJ*, 300, 522
 Chiang, J., & Romani, R. W. 1992, *ApJ*, 400, 629
 Daugherty, J. K., & Harding, A. K. 1982, *ApJ*, 252, 337
 Daugherty, J. K., & Harding, A. K. 1996, *ApJ*, 458, 278
 Harding, A. K., Tadamaru, E., & Esposito, L. S. 1978, *ApJ*, 225, 226
 Hirotani, K., & Okamoto, I. 1998, *ApJ*, 497, 563
 Hirotani, K., & Shibata, S. 1999a, *MNRAS* 308, 54 (Paper I)
 Hirotani, K., & Shibata, S. 1999b *MNRAS* 308, 67 (Paper II)
 Hirotani, K., & Shibata, S. 1999c, *PASJ* 51, 683 (Paper III)
 Romani, R. W. 1996, *ApJ*, 470, 469
 Sturmer, S. J., Dermer, C. D., & Michel, F. C. 1995, *ApJ*, 445, 736
 Zhang, L., & Cheng, K. S. 1997, *ApJ*, 487, 370